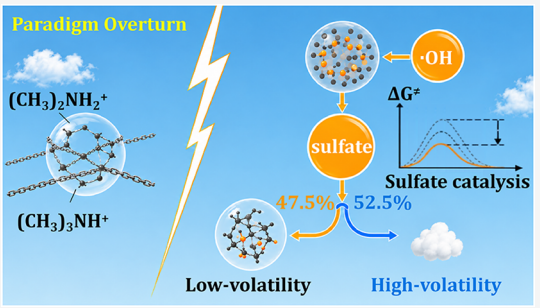
JACS
JOURNAL OF THE AMERICAN CHEMICAL SOCIETY
pubs.acs.org/JACS
Article

Particulate Amine Salts as Dynamic Hubs for Atmospheric Nitrogen Exchange

Weina Zhang, Jiale Lao, Shangyu Zhu, Yuemeng Ji, Guiying Li, Jie Zhong, Joseph S. Francisco,* and Taicheng An*

Cite This: https://doi.org/10.1021/jacs.6c10698
Read Online
ACCESS | Metrics & More | Article Recommendations | Supporting Information

ABSTRACT: Amine salts in atmospheric particulate matter have long been regarded as chemically inert and nonvolatile sinks for organic nitrogen. Here, we overturn this paradigm by demonstrating that these salts instead serve as dynamic hubs for nitrogen exchange. By using integrated ab initio calculations and high-resolution mass spectrometry, we show that dimethylamine (DMA) and trimethylamine (TMA) salts are efficiently initiated by •OH, generating reactive radical cation intermediates, which is not considered in previous organic nitrate chemistry. Meanwhile, sulfates dramatically accelerate the subsequent oxidation process by lowering free energy barriers by orders of magnitude compared to water-mediated pathways. Quantitative branching ratios reveal a bifurcated fate for oxidized amine salts: over 47.5% yields low-volatility amides (CH_2NCHO and $(CH_3)_2NCHO$) that preferentially remain in the particle phase, and the remaining 52.5% produces volatile species (CH_3NH_2 and CH_3NC) that partition to the gas phase. The latter branch is a previously unrecognized nitrogen re-release source, which explains the missing sources of HCN in remote background and amide in aged particles. These findings fundamentally revise the role of particulate amine salts in atmospheric organic nitrogen budgets, long-range transport, and nitrogen deposition in remote ecosystems.



1. INTRODUCTION

Atmospheric nitrogen cycling regulates climate forcing, ecosystem productivity, and air quality.[1−3] The organic nitrogen fraction represents a major, yet dynamically evolving component of this cycle, whose transformations directly impact atmospheric composition.[4,5] Small alkylamines, such as methylamine (MA), dimethylamine (DMA), and trimethylamine (TMA), constitute a critical class of these reactive organic nitrogen species, emitted from abundant marine, agricultural, and anthropogenic sources.[6−8] Gaseous alkylamines prefer to enter into fine particulates in the formation of particulate amine salts upon neutralization with ubiquitous acidic compounds like sulfuric acid or replacement with inorganic ammonia salts.[9−11] In conventional models, these particulate amine salts are considered chemically inert and thus set as a nitrogen sink, effectively removing nitrogen through particle deposition from active atmospheric chemistry.[12,13]

Yet, this view of amine salts as inert components is difficult to reconcile with atmospheric observations. Specifically, oxidized organic nitrogen compounds like amides are consistently found in aged particles, yet their formation pathways are not fully explained.[14,15] At the same time, stable background concentrations of volatile nitriles, such as hydrogen cyanide (HCN), persist in the clean remote atmosphere, indicating a missing and widespread source.[16,17] Together, these observations point to an unrecognized chemical process capable of reprocessing condensed-phase nitrogen and releasing a portion of it back to the gas phase.

Crucially, recent evidence suggests that amine salts are not the inert species they were assumed to be. For instance, oxidation of TMA salts in fine particles yields dominant products such as hydrogen cyanide (HCN) and amides, which is observed in the lab.[18] More recently, our work uncovered a potent atmospheric activation pathway, showing that gaseous hydroxyl radicals (•OH) can initiate the oxidation of MA salts, with sulfate (SO_4^{2-}) playing an indispensable catalytic role.[19] These findings establish that amine salts possess a previously unrecognized chemical reactivity under ambient conditions, with the potential to generate both gas- and particle-phase nitrogen products. Considering their widespread presence in particulates, this might explain the missing process implied by atmospheric observations.[12,20]

Here, we test the atmospheric implications of this reactivity by investigating the OH oxidation of two amine salts with higher abundance and more complex structures, namely, DMA and

Received: May 25, 2026
Revised: September 18, 2026
Accepted: September 21, 2026

ACS Publications
© XXXX American Chemical Society

Downloaded from pubs.acs.org/jacsat/article-pdf/doi/10.1021/jacs.6c10698/6872891/1/jacs.6c10698.pdf by GUANGDONG UNIV OF TECHNOLOGY user on 12 October 2026

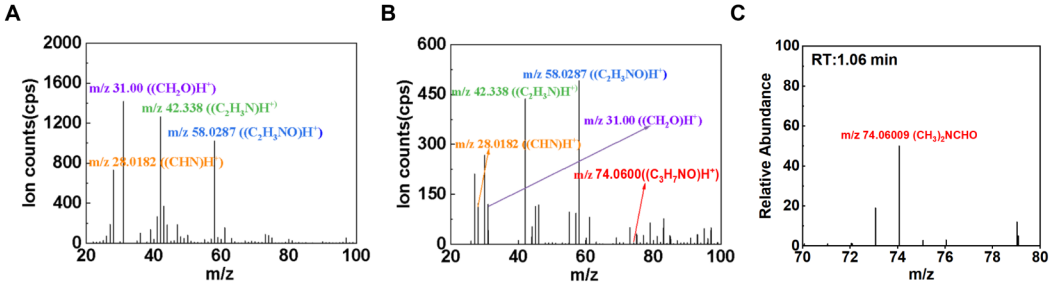


Figure 1. Oxidation products of DMA and TMA salts confirmed by (A–B) PTR-TOF-MS-1000 and (C) LC-Q-Orbitrap-MS/MS.

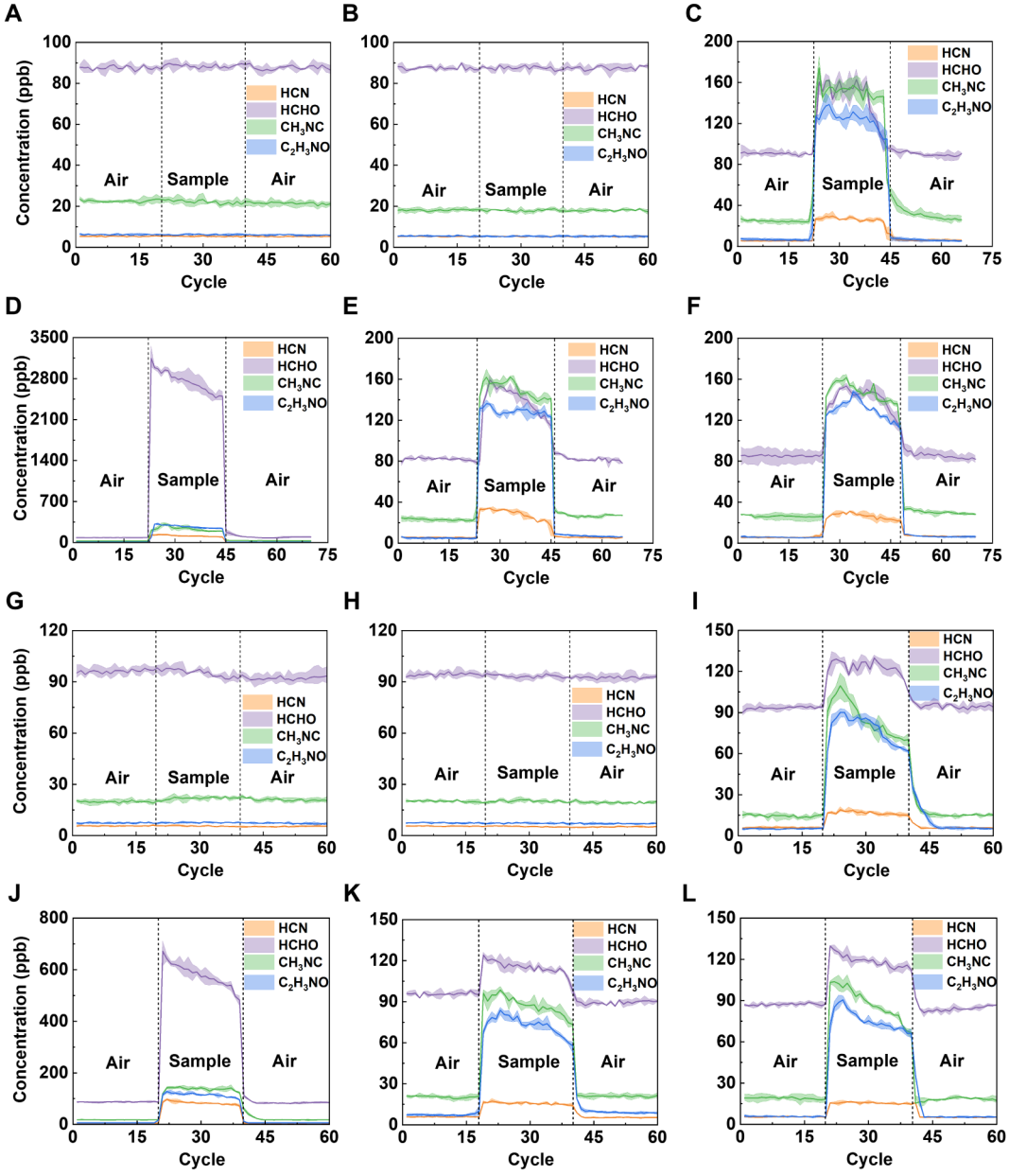


Figure 2. Product distributions of (A–F) DMA and (G–L) TMA salts detected by PTR-QMS under six different conditions: (A, G) no oxidant or anion, (B, H) sulfate only, (C, I) H_2O_2 only, (D, J) H_2O_2 + sulfate, (E, K) H_2O_2 + chloride, and (F, L) H_2O_2 + nitrate.

TMA salts. Using a combination of advanced mass spectrometry and ab initio calculations, we provide direct evidence that a significant portion of the nitrogen is recycled back to the gas phase as volatile nitriles, while the remainder contributes to nitrogen-enriched oxidized particles. This work redefines particulate amine salts from static sinks to dynamic exchange hubs in the atmospheric nitrogen cycle, resolving reported observational inconsistencies.

https://doi.org/10.1021/jacs.6c10698
J. Am. Chem. Soc. XXXX, XXX, XXX−XXX

Downloaded from pubs.acs.org/jacsat/article-pdf/doi/10.1021/jacs.6c10698/6872891/1/jacs.6c10698.pdf by GUANGDONG UNIV OF TECHNOLOGY user on 12 October 2026

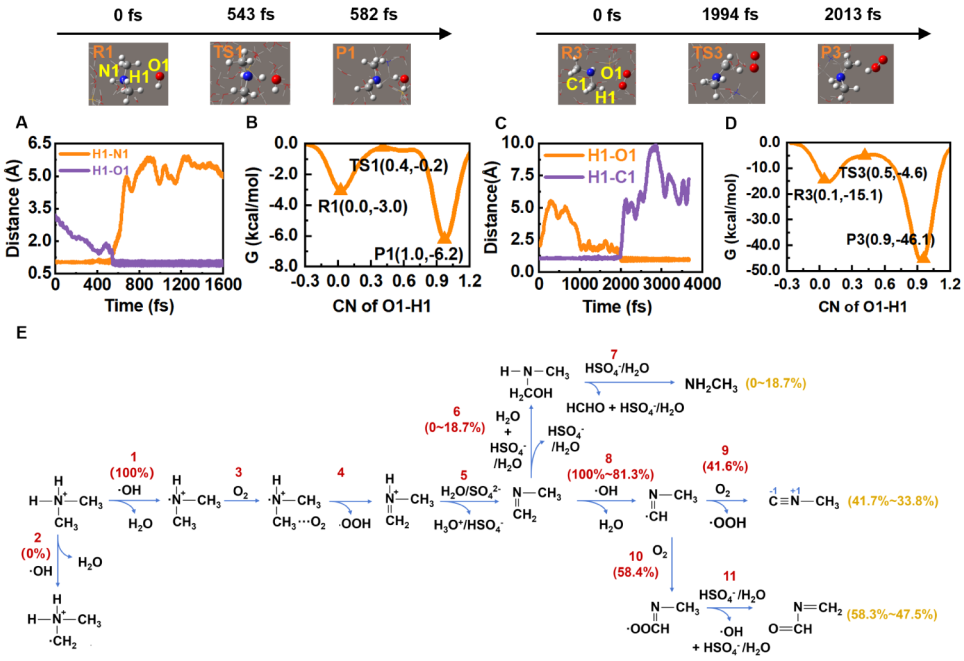


Figure 3. Oxidation activation mechanisms of DMA salt. (A–D) Intermediate formation processes, and (E) complete oxidation pathways for DMA salt systems. (A, C) Key bond distance evolutions from BOMD calculations. (B, D) Free energy profiles obtained by MTD calculations. R, TS, and P represent reactant, transition state, and product. Red values denote branching ratios of elementary pathways, and yellow values indicate product yields of multi-step reactions.

2. METHODS

2.1. Mass Spectrometry Experiments

To investigate the oxidation products of DMA salt and TMA salt, we designed six experimental conditions (Tables S1–S2). For each condition, equimolar DMA/TMA and hydrochloric acid were added to ensure the complete protonation of amines. The initial concentrations were 1 M for the DMA salt, 1 M for the TMA salt, and 0.5 M for H_2O_2. The sulfate concentration used in the catalytic experiments was 0.1 M, while the control experiments with chloride and nitrate were performed at matching concentrations of 0.1 M. Solution pH was maintained between 4 and 6 across all experiments to reflect the acidity of ambient fine particulate matter.[21] Products were quantified from the headspace gas of volumetric flasks under the reaction conditions of natural light (Figure S1). Initial product screening was performed using proton-transfer-reaction time-of-flight mass spectrometry (PTR-TOF-MS-1000, Ionicon Analytik, Innsbruck, Austria). Quantitative analysis was then conducted using proton-transfer-reaction quadrupole mass spectrometry (PTR-QMS-300, Ionicon Analytik, Innsbruck, Austria). Operating principles and technical specifications of both instruments have been detailed previously.[22,23] For TMA salt oxidation, a low-volatility product was not detectable by gas-phase mass spectrometry. We therefore used an ultrahigh-resolution hybrid quadrupole-Orbitrap mass spectrometer (Q Exactive HF, Thermo Fisher Scientific) coupled with liquid chromatography (LC-Q-Orbitrap-MS/MS) to analyze the liquid phase and confirm its formation.

2.2. Theoretical Calculations

To elucidate the activation mechanisms and subsequent oxidation pathways of DMA and TMA salts in sulfate-containing particulate matter, we performed Born–Oppenheimer molecular dynamics (BOMD) and metadynamics (MTD) simulations using the CP2K package.[24–26] Model systems were constructed as spherical droplets (Figure S2), containing 191 water molecules, one sulfate ion, and two DMA or TMA cations. Calculations employed the Becke-Lee-Yang-Parr exchange-correlation functional with Grimme's dispersion correction (BLYP-D3) to accurately describe weak interactions.[27] Valence electrons were treated with double-ζ plus polarization (DZVP) basis sets, while core electrons were represented by Goedecker–Teter–Hutter (GTH) norm-conserving pseudopotentials.[28,29]

Each system was equilibrated through geometry optimization under the NVT ensemble (constant atom number, volume, and temperature). Dynamics simulations were performed at 298 K using the Nosé–Hoover thermostat. After obtaining $\Delta G^{\neq}$ from MTD simulations, reaction rate constants (k) were derived using transition state theory combined with the Arrhenius equation. Branching ratios of each final product were calculated based on k and reported concentrations of each reactant in particulate matter. Additional experimental and computational details are provided in Supporting Information (SI).

3. RESULTS AND DISCUSSION

3.1. Oxidation Products of Amine Salts

We first characterized the oxidation products of DMA and TMA salts by using PTR-TOF-MS. In solutions containing DMA or TMA salts with H_2O_2, we detected aldehydes (CH_2NCHO and HCHO) and cyan compounds (CH_3NC and HCN) (Figure 1A–B). For TMA salt solutions, a weak signal at m/z = 74.0600 suggested the formation of *N*,*N*-dimethylformamide (DMF, $(CH_3)_2NCHO$)). Subsequent LC-Q-Orbitrap-MS/MS analysis confirmed DMF production, with a distinct peak at retention time 1.06 min (Figure 1C). In contrast, our previous results showed that MA salt oxidation yielded only HCHO and HCN.[19] The greater diversity of oxidation products from DMA and TMA salts suggests that these larger amine salts undergo different oxidation pathways compared with MA salts.

To quantify the role of •OH in these oxidation reactions, we employed PTR-QMS to compare product distributions under six different conditions (Tables S1–S2): (1) no oxidant or anion (Exp. 1 and Exp. 7), (2) sulfate only (Exp. 2 and Exp. 8), (3) H_2O_2 only (Exp. 3 and Exp. 9), (4) H_2O_2 + sulfate (Exp. 4 and Exp. 10), (5) H_2O_2 + chloride (Exp. 5 and Exp. 11), and (6) H_2O_2 + nitrate (Exp. 6 and Exp. 12). Under control or sulfate-only conditions, product concentrations from both amine salts were indistinguishable from background air (Figure 2A–B, G–

https://doi.org/10.1021/jacs.6c10698
J. Am. Chem. Soc. XXXX, XXX, XXX–XXX

Downloaded from pubs.acs.org/jacsat/article-pdf/doi/10.1021/jacs.6c10698/6872891/jacs.6c10698.pdf by GUANGDONG UNIV OF TECHNOLOGY user on 12 October 2026

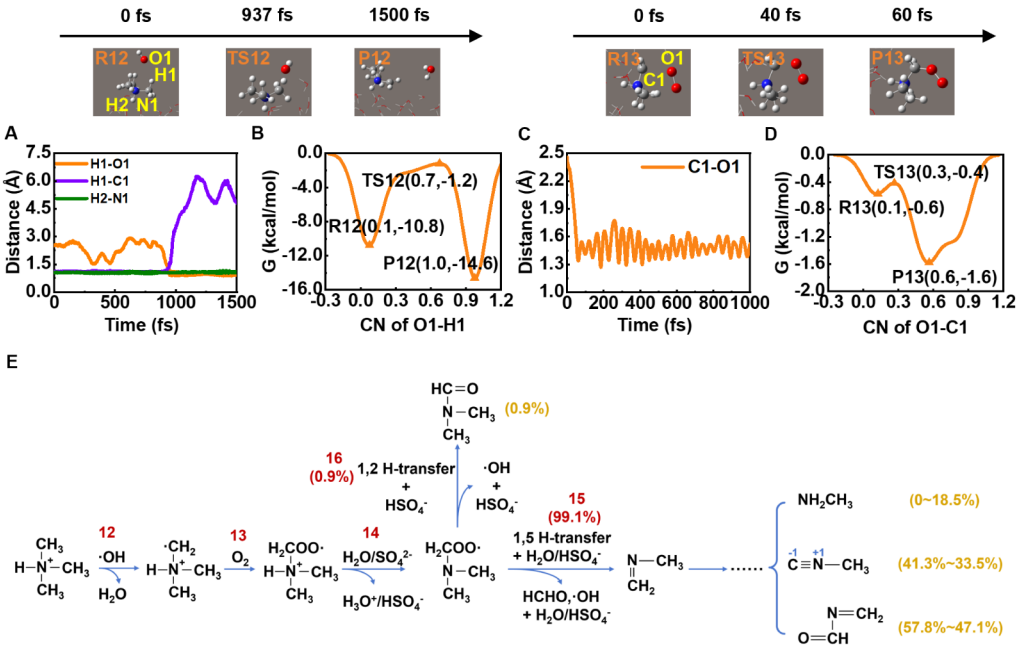


Figure 4. Oxidation activation mechanisms of TMA salt. (A–D) Intermediate formation processes, and (E) complete oxidation pathways for TMA salt systems. (A, C) Key bond distance evolutions from BOMD calculations. (B, D) Free energy profiles obtained by MTD calculations. R, TS, and P represent reactant, transition state, and product. Red values denote branching ratios of elementary pathways, and yellow values indicate product yields of multi-step reactions.

H). However, upon addition of H_2O_2 alone, all product concentrations increased by tens of parts per billion (ppb) (Figure 2C and I), confirming that •OH initiates amine salt oxidation.

Strikingly, when sulfate was present together with H_2O_2, product concentrations increased dramatically by two to three orders of magnitude for DMA salts (from tens to hundreds or thousands of ppb) and by one order of magnitude for TMA salts (to hundreds of ppb) (Figure 2D and J). This enhancement demonstrates that sulfate specifically promotes the •OH-initiated oxidation of amine salts. Notably, HCHO production from TMA salts was an order of magnitude lower than from DMA salts. Given that DMF was uniquely identified as a TMA oxidation product, we attribute this difference to competitive partitioning between DMF-forming and HCHO-forming pathways. Moreover, replacing sulfate with chloride or nitrate in the presence of H_2O_2 yielded product concentrations like those with H_2O_2 alone (Figure 2E–F and K–L). This indicated that the increase in the product when sulfate was present was not caused by ionic strength effects or salting-out phenomena. Thus, chloride and nitrate salts do not promote amine salt oxidation, highlighting the unique catalytic role of sulfate in this chemistry.

Considering that H_2O_2 might directly oxidize DMA salt and TMA salt, we conducted control experiments under the same conditions as Exp. 4 and Exp. 10, with the addition of DMPO, a well-established •OH radical scavenger (Table S3, Exp. 13 and Exp. 14). 5,5-Dimethyl-1-pyrroline *N*-oxide (DMPO) was added after complete protonation of DMA and TMA, followed by the addition of H_2O_2 and sulfate. The detected product compositions are the same as those in the presence of tert-butanol, but their concentrations (Figure S3A–B) were 1–2 orders of magnitude lower than those without the scavenger (Figure 2D and J). This result confirms that H_2O_2 alone cannot directly oxidize the amine salts to the observed products; instead, the reactive species responsible is •OH generated from H_2O_2. Meanwhile, theoretical calculations were employed to verify whether H_2O_2 could directly react with DMA salt and TMA salt. The calculated trajectories (Figure S3C–D) show that H_2O_2 and the amine salts briefly approach each other and then rapidly separate, without any tendency to react. This confirms that H_2O_2 cannot directly participate in the oxidation of DMA salt and TMA salt, consistent with the experimental observations.

3.2. Activation Mechanism of Amine Salt Oxidation

Experimental analysis revealed different oxidation products for DMA and TMA salts (Figure 1), suggesting distinct reactive intermediates and pathways. We combined BOMD and MTD calculations to elucidate the activation mechanisms for both systems. In DMA salt activation, BOMD trajectories showed that •OH abstracts a hydrogen atom from the amine group of DMA salt (Reaction 1), producing the amine radical cation $(CH_3)_2NH^+$• (Figure 3A). No trajectories showed formation of the alternative methyl radical cation $•CH_2NH_2CH_3^+$ (Reaction 2). MTD calculations explained this selectivity: free energy barrier ($\Delta G^{\neq}$) for Reaction 1 (Figure 3B) is 4.2 kcal mol^{-1} lower than for Reaction 2 (Figure S4). This barrier difference corresponds to a rate constant three orders of magnitude higher, yielding a 100% branching ratio for $(CH_3)_2NH^+$• formation. The $(CH_3)_2NH^+$• intermediate subsequently reacts with interfacial O_2 through a barrierless process, forming complex $(CH_3)_2NH^+•\cdots O_2$ (Reaction 3; Figure 3C). This complex has a lifetime of only ~1000 fs before decomposing into the *N*-methylmethaniminium cation ($CH_3NHCH_2^+$) and $•HO_2$ (Reaction 4). The calculated $\Delta G^{\neq}$ for this decomposition is 10.5 kcal mol^{-1} (Figure 3D), yielding a rate constant of 1.24×10^5 M^{-1} s^{-1}. Unlike the parent DMA salt ($DMAH^+$), the $CH_3NHCH_2^+$ cation undergoes deprotonation with sulfate (Figure S5A), generating *N*-methylmethanimine (CH_3NCH_2) as a first-generation oxidation product (Reaction 5). This matches one of the major products identified by PTR-TOF-MS

https://doi.org/10.1021/jacs.6c10698
J. Am. Chem. Soc. XXXX, XXX, XXX–XXX

Downloaded from pubs.acs.org/jacsat/article-pdf/doi/10.1021/jacs.6c10698/6872891/1/jacs.6c10698.pdf by GUANGDONG UNIV OF TECHNOLOGY user on 12 October 2026

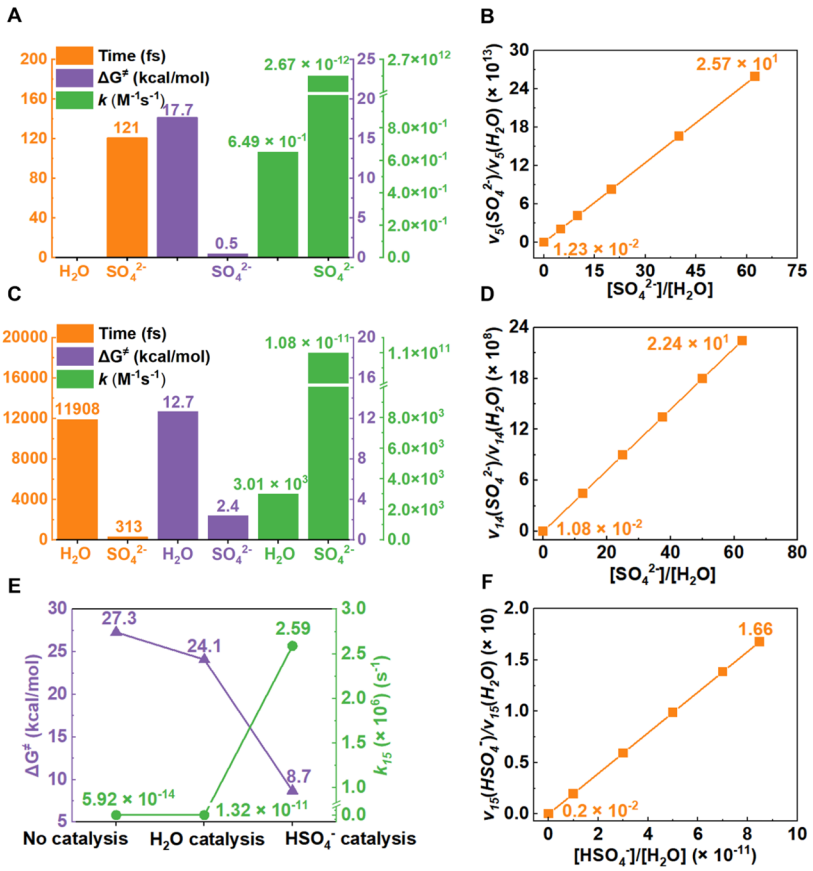


Figure 5. Sulfate contribution to the first-generation product formation in the (A−B) DMA salt system and the (C−F) TMA salt system. Left panel displays the reaction time, $\Delta G^{\neq}$ and k under different catalysis conditions, and right panel displays corresponding yield rate changes.

in the DMA system (Figure 1A). CH_3NCH_2 then undergoes further oxidation (Reactions 6−11, Figures S6−S8), ultimately yielding methyl isocyanide (CH_3NC) and *N*-methylenemethanimine (CH_2NCHO) as major second-generation products, consistent with experimental observations (Figure 1A). In this DMA activation mechanism (Figure 3E), $(CH_3)_2NH^+\bullet$ and $(CH_3)_2NH^+\bullet\cdots O_2$ serve as key reactive intermediates.

$$(CH_3)_2NH_2^+ + \bullet OH \rightarrow (CH_3)_2NH^+\bullet + H_2O \quad (1)$$

$$(CH_3)_2NH_2^+ + \bullet OH \rightarrow \bullet CH_2NH_2CH_3^+ + H_2O \quad (2)$$

$$(CH_3)_2NH^+\bullet + O_2 \rightarrow (CH_3)_2NH^+\bullet\cdots O_2 \quad (3)$$

$$(CH_3)_2NH^+\bullet\cdots O_2 \rightarrow CH_3NHCH_2^+ + \bullet HO_2 \quad (4)$$

$$CH_3NHCH_2^+ + SO_4^{2-}/H_2O \rightarrow CH_3NCH_2 + HSO_4^-/H_3O^+ \quad (5)$$

$$CH_3NCH_2 + H_2O + HSO_4^-/H_2O \rightarrow CH_3NHCH_2OH + HSO_4^-/H_2O \quad (6)$$

$$CH_3NHCH_2OH + HSO_4^-/H_2O \rightarrow NH_2CH_3 + HCHO + HSO_4^-/H_2O \quad (7)$$

$$CH_3NCH_2 + \bullet OH \rightarrow CH_3NCH\bullet + H_2O \quad (8)$$

$$CH_3NCH\bullet + O_2 \rightarrow CH_3NC + \bullet HO_2 \quad (9)$$

$$CH_3NCH\bullet + O_2 \rightarrow CH_3NCHOO\bullet \quad (10)$$

$$CH_3NCHOO\bullet + HSO_4^-/H_2O \rightarrow CH_2NCHO + \bullet OH + HSO_4^-/H_2O \quad (11)$$

In TMA salt activation, unlike DMA salt, which forms nitrogen-centered radical cations, TMA salt thus produces carbon-centered radical cations. Here, •OH abstracts a hydrogen atom exclusively from a methyl group (Reaction 12), generating the carbon-centered radical cation $(CH_3)_2NHCH_2^+\bullet$ (Figure 4A). MTD calculations gave a $\Delta G^{\neq}$ of 9.6 kcal mol^{-1} for this reaction (Figure 4B), indicating rapid kinetics under atmospheric conditions. Electrostatic potential maps explain this divergence: the methyl groups of TMA salt exhibit higher electrostatic potential than the amine group, suggesting stronger attraction by •OH, whereas DMA salt shows the opposite distribution (Figure S9A−B). The $(CH_3)_2NHCH_2^+\bullet$ intermediate undergoes direct addition with O_2 (Reaction 13), forming a cationic peroxy radical $(CH_3)_2NHCH_2OO^+\bullet$ (Figure 4C). MTD calculations gave a $\Delta G^{\neq}$ of 0.2 kcal mol^{-1} for this addition (Figure 4D), implying rapid kinetics under ambient conditions. In contrast to the DMA pathway, where $(CH_3)_2NH^+\bullet\cdots O_2$ decomposes before deprotonation (Reaction 4), the $(CH_3)_2NHCH_2OO^+\bullet$ intermediate undergoes direct deprotonation by SO_4^{2-} (Figure S10A−B) or H_2O (Figure S10C−D), yielding the peroxy radical $(CH_3)_2NCH_2OO\bullet$ (Reaction 14). This peroxy radical then undergoes hydrogen shift reactions catalyzed by HSO_4^-/H_2O, producing first-generation products including CH_3NCH_2 and

https://doi.org/10.1021/jacs.6c10698
J. Am. Chem. Soc. XXXX, XXX, XXX−XXX

Downloaded from pubs.acs.org/jacsat/article-pdf/doi/10.1021/jacs.6c10698/6872891/1/jacs.6c10698.pdf by GUANGDONG UNIV OF TECHNOLOGY user on 12 October 2026

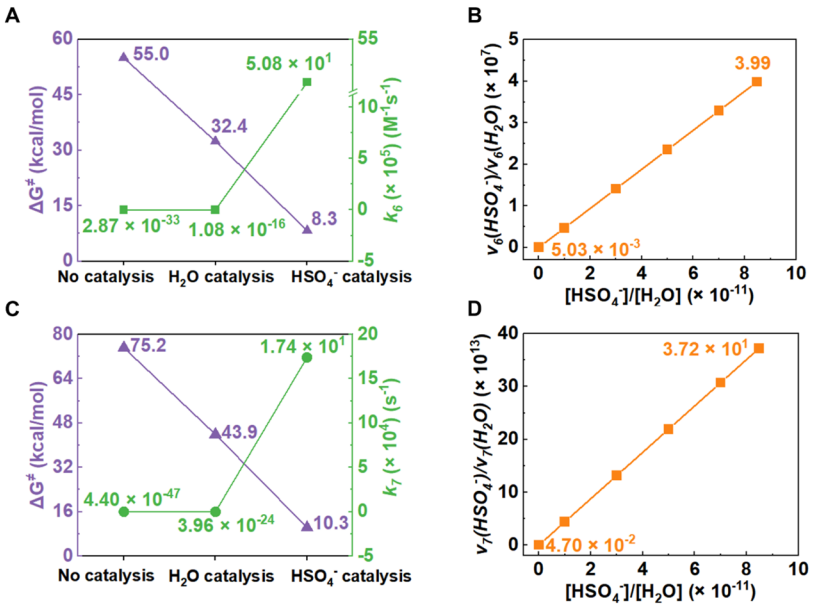


Figure 6. Sulfate contribution to the second-generation product formation, specifically (A–B) CH_3NHCH_2OH, (C–D) HCHO, and NH_2CH_3. Left panel displays $\Delta G^{\neq}$ and k under different catalysis conditions, and right panel displays corresponding yield rate changes.

HCHO (Reaction 15, Figure S11A–C), as well as *N*,*N*-dimethylformamide (DMF, $(CH_3)_2NCHO$) (Reaction 16, Figure S11D). CH_3NCH_2 undergoes further oxidation to yield the same second-generation products observed in DMA salt systems (Reactions 6–11), including CH_3NC and CH_2NCHO (Figure 1A–B). Notably, DMF forms exclusively in the TMA salt system, consistent with LC-Q-Orbitrap-MS/MS analyses (Figure 1C). In summary, TMA oxidation (Figure 4E) proceeds through two key intermediates: the carbon-centered radical cation $(CH_3)_2NHCH_2^+\bullet$ and the cationic peroxy radical $(CH_3)_2NHCH_2OO^+\bullet$. The distinct electronic structures of these intermediates, compared to those in the DMA salt system, explain the divergent product distributions observed experimentally.

$$(CH_3)_3NH^+ + \bullet OH \rightarrow (CH_3)_2NHCH_2^+\bullet + H_2O \quad (12)$$

$$(CH_3)_2NHCH_2^+\bullet + O_2 \rightarrow (CH_3)_2NHCH_2OO^+\bullet \quad (13)$$

$$(CH_3)_2NHCH_2OO^+\bullet + SO_4^{2-}/H_2O \rightarrow (CH_3)_2NCH_2OO\bullet + HSO_4^-/H_3O^+ \quad (14)$$

$$(CH_3)_2NCH_2OO\bullet + HSO_4^-/H_2O \rightarrow CH_3NCH_2 + HCHO + HSO_4^-/H_2O \quad (15)$$

$$(CH_3)_2NCH_2OO\bullet + HSO_4^- \rightarrow (CH_3)_2NCHO + \bullet OH + HSO_4^- \quad (16)$$

3.3. Promoting Effect of Sulfate on Product Formation

PTR-QMS results show that sulfate plays a unique role in promoting product formation of amine salts (Figure 2), which are not found in nitrate or chloride. Hence, we quantify the promoting effect derived from sulfates (SO_4^{2-} and HSO_4^-) based on the proposed oxidation mechanism above. In the DMA salt system, CH_3NCH_2 forms via deprotonation of $CH_3NHCH_2^+$ (Reaction 5). BOMD simulations showed that with SO_4^{2-} participation, this reaction completes within 121 fs (Figure S5A). In contrast, BOMD simulations with H_2O alone did not succeed, suggesting a high energy barrier.[30] MTD calculations confirmed this: the free energy barrier with SO_4^{2-} is 12.7 kcal mol^{-1} lower than with H_2O (Figure S5B–C; Figure 5A). This difference corresponds to a rate constant 13 orders of magnitude higher for the sulfate-mediated pathway. In the ambient atmosphere, the competition between these pathways depends on the $[SO_4^{2-}]/[H_2O]$ ratio in particulate matter, with $v_5(SO_4^{2-})/v_5(H_2O) = \{k_5(SO_4^{2-})[SO_4^{2-}]\}/\{k_5(H_2O)[H_2O]\}$. Given typical $[SO_4^{2-}]/[H_2O]$ ratios of 0.03–62.5 in PM,[31,32] the competitive ratio ranges from 1.23×10^{11} to 2.57×10^{14} (Figure 5B). Thus, SO_4^{2-} overwhelmingly dominates CH_3NCH_2 formation in the DMA system.

In the TMA salt system, CH_3NCH_2 formation proceeds through two steps: deprotonation of $(CH_3)_2NHCH_2OO^+\bullet$ (Reaction 14) followed by a 1,5 H-shift of $(CH_3)_2NCH_2OO\bullet$ (Reaction 15). Both sulfate (SO_4^{2-} and HSO_4^-) and water can participate in each step. For Reaction 14, BOMD showed deprotonation with SO_4^{2-} completes in 313 fs (Figure S10A), which is less than 3% of the time required with H_2O (Figure S10C). MTD calculations gave a $\Delta G^{\neq}$ of only 2.4 kcal mol^{-1} with SO_4^{2-}, corresponding to $k = 1.08 \times 10^{11}$ M^{-1} s^{-1}, which is eight orders of magnitude higher than with H_2O (Figure 5C). The resulting competitive ratio $v_{14}(SO_4^{2-})/v_{14}(H_2O)$ ranges from 1.08×10^6 to 2.24×10^9 (Figure 5D). For Reaction 15, MTD calculations compared uncatalyzed, water-catalyzed, and HSO_4^--catalyzed pathways (Figure S11A–C). The free energy barriers are 27.3, 24.1, and 8.7 kcal mol^{-1}, respectively (Figure 5E). HSO_4^- catalysis thus enables the most facile reaction. Based on rate constants and ambient $[HSO_4^-]/[H_2O]$ ratios (1.07×10^{-13} to 8.48×10^{-11}),[31] the competitive ratio $v_{15}(HSO_4^-)/v_{15}(H_2O) = \{k_{15}(HSO_4^-)[HSO_4^-]\}/\{k_{15}(H_2O)[H_2O]\}$ ranges from 0.02 to 16.6 (Figure 5F), indicating that both HSO_4^- and H_2O jointly dominate CH_3NCH_2 formation in the TMA salt system. Similarly, HSO_4^- catalyzes the 1,2 H-shift of $(CH_3)_2NCH_2OO\bullet$ (Reaction 16, Figure S11D), producing the unique first-generation product DMF. Collectively, sulfate

Downloaded from pubs.acs.org/jacsat/article-pdf/doi/10.1021/jacs.6c10698/6872891/jacs.6c10698.pdf by GUANGDONG UNIV OF TECHNOLOGY user on 12 October 2026

https://doi.org/10.1021/jacs.6c10698
J. Am. Chem. Soc. XXXX, XXX, XXX–XXX

(SO_4^{2-} and HSO_4^-) substantially promotes first-generation product formation in both amine salt systems.

We further found that HSO_4^- continues to accelerate second-generation product formation. For the hydration of CH_3NCH_2 to CH_3NHCH_2OH (Reaction 6), MTD calculations compared uncatalyzed, water-based catalyzed, and HSO_4^--catalyzed pathways (Figure S6A–C). The free energy barriers are 55.0, 32.4, and 8.3 kcal mol^{-1}, respectively, corresponding to rate constants increasing from 2.87×10^{-28} to 5.08×10^6 M^{-1} s^{-1} (Figure 6A). HSO_4^- thus enables this reaction to proceed rapidly under ambient conditions. Based on rate constants and ambient $[HSO_4^-]/[H_2O]$ ratios,[31] the competitive ratio $v_6(HSO_4^-)/v_6(H_2O)$ ranges from 5.03×10^4 to 3.99×10^7 (Figure 6B), demonstrating that HSO_4^- dominates CH_3NHCH_2OH formation in PM. Similarly, for the decomposition of CH_3NHCH_2OH to HCHO and methylamine (NH_2CH_3) (Reaction 7), MTD results (Figure S6D–F) showed the lowest $\Delta G^{\neq}$ (10.3 kcal mol^{-1}) and highest k (1.74×10^5 s^{-1}) under HSO_4^- catalysis (Figure 6C). The competitive ratio $v_7(HSO_4^-)/v_7(H_2O)$ ranges from 4.70×10^{11} to 3.72×10^{14} (Figure 6D), confirming that HSO_4^- consistently dominates the formation of these oxidation products.

The formation of CH_2NCHO (Reaction 11) presents an exception. Comparison of uncatalyzed, water-catalyzed, and HSO_4^--catalyzed pathways (Figure S8D) showed that HSO_4^- significantly lowers the energy barrier to 6.2 kcal mol^{-1}, which is less than half that of water-catalyzed or uncatalyzed pathways. This yields $k = 1.76 \times 10^8$ s^{-1}, seven orders of magnitude higher than uncatalyzed or water-catalyzed reactions. However, given ambient $[HSO_4^-]/[H_2O]$ ratios[31] of 1.07×10^{-13} to 8.48×10^{-11}, the competitive ratio $v_{11}(HSO_4^-)/v_{11}(H_2O)$ ranges from 5.04×10^{-7} to 3.99×10^{-4} (Figure S8E). Thus, in contrast to other products, H_2O instead dominates CH_2NCHO formation in ambient PM.

Considering that the concentration of SO_4^{2-} in real sulfate-containing particulate matter is much higher than that of HSO_4^-,[33,34] this might lead to the oxidation of DMA salt and TMA salt being predominantly catalyzed by SO_4^{2-} rather than HSO_4^- in the processes of Reactions 6, 7, 11, 15, and 16. To confirm this possibility, we performed additional theoretical calculations to examine whether SO_4^{2-} could participate in the catalytic effect. If SO_4^{2-} was involved in the catalytic reaction, in Reaction 6 it would abstract H from the adjacent H_2O in Reaction 6 or from the −OH group of the amine salt in Reactions 7, 11, 15, and 16, forming HSO_4^-. However, the BOMD results show that SO_4^{2-} does not abstract H from H_2O or −OH group in Reactions 6, 11, and 15 (Figure S12A, C, and D). Specifically, in Reaction 7, SO_4^{2-} first abstracts H from H_3O^+ via a water bridge, forming HSO_4^- (Figure S12B). Then, HSO_4^- acts as catalysis promotes latter reaction. Therefore, SO_4^{2-} cannot directly engage in Reactions 6–7, 11, and 15. Therefore, although HSO_4^- is present only in trace amounts at pH 6, it plays a unique and indispensable catalytic role in promoting amine salt conversion.

In summary, sulfate drives the formation and transformation of both first- and second-generation oxidation products in amine salt systems. This catalytic role explains the dramatic increase in product concentrations observed by PTR-QMS upon introduction of SO_4^{2-} to DMA and TMA salt systems (Figure 2D and J). In general sulfate concentration in atmospheric particles, we quantified the ultimate product branching ratios for both amine salt oxidations. In the DMA salt oxidation, oxidation ultimately yields CH_3NH_2, CH_3NC, and CH_2NCHO with branching ratios of 0–18.7%, 41.7%–33.8%, and 58.3–47.5%, respectively (Figure 3E). The TMA salt oxidation follows a distinct pathway due to the formation of $(CH_3)_2NCHO$ as an additional branch, yielding final branching ratios of 0.9% for $(CH_3)_2NCHO$, 0–18.5% for CH_3NH_2, 41.3–33.5% for CH_3NC, and 57.8–47.1% for CH_2NCHO (Figure 4E). Based on their Henry's law constants, CH_3NH_2 and CH_3NC are volatile species ($H_S < 10^{-3}$ mol m^{-3} Pa^{-1}), while CH_2NCHO and $(CH_3)_2NCHO$ are low-volatility amides ($H_S > 10^2$ mol m^{-3} Pa^{-1}).[35] Thus, of the oxidized amine salt, 58.3–47.5% of the DMA products and 58.7–48.0% of the TMA products ($(CH_3)_2NCHO$ and CH_2NCHO) are expected to stay in the particle phase,[36,37] while the remaining 41.7–52.5% and 41.3–52.0% will likely escape to the gas phase. Notably, CH_3NH_2 undergoes further reactions to produce volatile species such as HCHO and HCN.[19]

4. CONCLUSION

Traditional models of atmospheric chemistry treat particulate amine salts as inert, permanent components of the particle phase. Our work reveals the opposite: that particulate amine salts can be activated under ambient conditions and be partially released into the atmosphere. Gas-phase •OH activates amine salts into reactive radical cation intermediates, which is a species previously not considered in the particle-phase chemistry. In their subsequent conversion, sulfate plays a unique and key catalytic role, which is not found in nitrate or chloride. Kinetically determined by the sulfate concentration of atmospheric particles, the fate of the amine salts bifurcates. For both DMA and TMA salts, more than 40% of the products escape as volatile CH_3NH_2 and CH_3NC, while the remainder forms low-volatility amides retained in particles. Therefore, we demonstrate that amine salts are dynamic hubs between the particle and gas phases rather than terminal sinks as treated in traditional atmospheric models.

This mechanism solves two long-standing puzzles about nitrogen sources: it provides a potential source of HCN in clean remote atmospheres (via produced CH_3NH_2 oxidation) and explains amide formation in aged particles. In addition, current models assume that 100% of the amine salt nitrogen contributes to particle mass growth. However, based on the proposed activation mechanism, more than 40% of the amine salt escapes as volatile compounds. Accordingly, the contribution of the amine salt to particle mass has been previously overestimated. For these reasons, the activation kinetic parameters of amine salts must be incorporated into the atmospheric nitrogen cycling models. This is also necessary for addressing relevant issues such as ecosystem productivity, air quality, and aerosol climate forcing.

■ ASSOCIATED CONTENT

Supporting Information

The Supporting Information is available free of charge at https://pubs.acs.org/doi/10.1021/jacs.6c10698.

Additional method details and supplementary figures, including computational details of the BOMD and MTD simulations, calculations of reaction rate constants and equilibrium constants, Tables S1–S2, and Figures S1–S9 (PDF)

Downloaded from pubs.acs.org/jacsat/article-pdf/doi/10.1021/jacs.6c10698/6872891/jacs.6c10698.pdf by GUANGDONG UNIV OF TECHNOLOGY user on 12 October 2026

https://doi.org/10.1021/jacs.6c10698
J. Am. Chem. Soc. XXXX, XXX, XXX–XXX

AUTHOR INFORMATION

Corresponding Authors

Joseph S. Francisco − *Department of Earth and Environmental Science and Department of Chemistry, University of Pennsylvania, Philadelphia, Pennsylvania 19104-6316, United States;* orcid.org/0000-0002-5461-1486; Email: frjoseph@sas.upenn.edu

Taicheng An − *China Guangdong-Hong Kong-Macao Joint Laboratory for Contaminants Exposure and Health, Guangdong Key Laboratory of Environmental Catalysis and Health Risk Control, Institute of Environmental Health and Pollution Control, Guangdong University of Technology, Guangzhou 510006, China; Guangdong Basic Research Center of Excellence for Ecological Security and Green Development, School of Environmental Science and Engineering, Guangdong University of Technology, Guangzhou 510006, China;* orcid.org/0000-0001-6918-8070; Email: antc99@gdut.edu.cn

Authors

Weina Zhang − *China Guangdong-Hong Kong-Macao Joint Laboratory for Contaminants Exposure and Health, Guangdong Key Laboratory of Environmental Catalysis and Health Risk Control, Institute of Environmental Health and Pollution Control, Guangdong University of Technology, Guangzhou 510006, China; Guangdong Basic Research Center of Excellence for Ecological Security and Green Development, School of Environmental Science and Engineering, Guangdong University of Technology, Guangzhou 510006, China*

Jiale Lao − *China Guangdong-Hong Kong-Macao Joint Laboratory for Contaminants Exposure and Health, Guangdong Key Laboratory of Environmental Catalysis and Health Risk Control, Institute of Environmental Health and Pollution Control, Guangdong University of Technology, Guangzhou 510006, China; Guangdong Basic Research Center of Excellence for Ecological Security and Green Development, School of Environmental Science and Engineering, Guangdong University of Technology, Guangzhou 510006, China*

Shangyu Zhu − *China Guangdong-Hong Kong-Macao Joint Laboratory for Contaminants Exposure and Health, Guangdong Key Laboratory of Environmental Catalysis and Health Risk Control, Institute of Environmental Health and Pollution Control, Guangdong University of Technology, Guangzhou 510006, China; Guangdong Basic Research Center of Excellence for Ecological Security and Green Development, School of Environmental Science and Engineering, Guangdong University of Technology, Guangzhou 510006, China*

Yuemeng Ji − *China Guangdong-Hong Kong-Macao Joint Laboratory for Contaminants Exposure and Health, Guangdong Key Laboratory of Environmental Catalysis and Health Risk Control, Institute of Environmental Health and Pollution Control, Guangdong University of Technology, Guangzhou 510006, China; Guangdong Basic Research Center of Excellence for Ecological Security and Green Development, School of Environmental Science and Engineering, Guangdong University of Technology, Guangzhou 510006, China;* orcid.org/0000-0002-8641-4276

Guiying Li − *China Guangdong-Hong Kong-Macao Joint Laboratory for Contaminants Exposure and Health, Guangdong Key Laboratory of Environmental Catalysis and Health Risk Control, Institute of Environmental Health and Pollution Control, Guangdong University of Technology, Guangzhou 510006, China; Guangdong Basic Research Center of Excellence for Ecological Security and Green Development, School of Environmental Science and Engineering, Guangdong University of Technology, Guangzhou 510006, China;* orcid.org/0000-0002-6777-4786

Jie Zhong − *School of Petroleum Engineering, China University of Petroleum (East China), Qingdao 266580, China;* orcid.org/0000-0003-4070-9383

Complete contact information is available at: https://pubs.acs.org/10.1021/jacs.6c10698

Author Contributions

The manuscript was written through contributions of all the authors.

Notes

The authors declare no competing financial interest.

ACKNOWLEDGMENTS

This work is supported by NSFC (22522602, 42277081, and 42077189), the Basic and Applied Basic Research Fund Project of Guangdong Province (2024A1515012691), the National Key Research and Development Program of China (2022YFC3105600), and the Guangzhou Science and Technology Program (2025A04J5188).

REFERENCES

(1) Schimel, D. S.; Braswell, B. H.; Parton, W. J. Equilibration of the terrestrial water, nitrogen, and carbon cycles. *Proc. Natl. Acad. Sci. U. S. A.* **1997**, *94* (16), 8280−8283.

(2) Mason, R. E.; Craine, J. M.; Lany, N. K.; Jonard, M.; Ollinger, S. V.; Groffman, P. M.; Fulweiler, R. W.; Angerer, J.; Read, Q. D.; Reich, P. B.; et al. Evidence, causes, and consequences of declining nitrogen availability in terrestrial ecosystems. *Science* **2022**, *376* (6590), No. eabh3767.

(3) Galloway, J. N.; Townsend, A. R.; Erisman, J. W.; Bekunda, M.; Cai, Z.; Freney, J. R.; Martinelli, L. A.; Seitzinger, S. P.; Sutton, M. A. Transformation of the Nitrogen Cycle: Recent Trends, Questions, and Potential Solutions. *Science* **2008**, *320* (5878), 889−892.

(4) Sun, J.; Fu, J. S.; Huang, K. Organic nitrates and other oxidized nitrogen compounds contribute significantly to the total nitrogen depositions in the United States. *Proc. Natl. Acad. Sci. U. S. A.* **2016**, *113* (31), No. E4433−E4434.

(5) Sun, X. S.; Fan, D. J.; Hu, L. M.; Wang, H. J. Global patterns and drivers of nitrogen isotope signal in modern marine sediments. *Nat. Commun.* **2025**, *16* (1), 13.

(6) Liu, M.; Wang, X.; Liu, Z.; Jiang, Y.; Li, M.; Zhang, J.; Sun, Y.; Zhu, Y.; Xue, L.; Wang, W. Characteristics and origins of fine particulate amines at a coastal mountain site in northern China in spring. *Atmos. Environ.* **2024**, *321*, 120365.

(7) Zhang, W.; Zhong, J.; Shi, Q.; Gao, L.; Ji, Y.; Li, G.; An, T.; Francisco, J. S. Mechanism for Rapid Conversion of Amines to Ammonium Salts at the Air−Particle Interface. *J. Am. Chem. Soc.* **2021**, *143* (2), 1171−1178.

(8) Ning, A.; Zhong, J.; Li, L.; Li, H.; Liu, J.; Liu, L.; Liang, Y.; Li, J.; Zhang, X.; Francisco, J. S.; et al. Chemical Implications of Rapid Reactive Absorption of I2O4 at the Air-Water Interface. *J. Am. Chem. Soc.* **2023**, *145* (19), 10817−10825.

(9) Liu, L.; Yu, F.; Du, L.; Yang, Z.; Francisco, J. S.; Zhang, X. Rapid sulfuric acid−dimethylamine nucleation enhanced by nitric acid in polluted regions. *Proc. Natl. Acad. Sci. U. S. A.* **2021**, *118* (35), No. e2108384118.

Downloaded from pubs.acs.org/jacsat/article-pdf/doi/10.1021/jacs.6c10698/6872891/jacs.6c10698.pdf by GUANGDONG UNIV OF TECHNOLOGY user on 12 October 2026

(10) Yao, L.; Garmash, O.; Bianchi, F.; Zheng, J.; Yan, C.; Kontkanen, J.; Junninen, H.; Mazon, S. B.; Ehn, M.; Paasonen, P.; et al. Atmospheric new particle formation from sulfuric acid and amines in a Chinese megacity. *Science* **2018**, *361* (6399), 278−281.
(11) Almeida, J.; Schobesberger, S.; Kürten, A.; Ortega, I. K.; Kupiainen-Määttä, O.; Praplan, A. P.; Adamov, A.; Amorim, A.; Bianchi, F.; Breitenlechner, M.; et al. Molecular understanding of sulphuric acid−amine particle nucleation in the atmosphere. *Nature* **2013**, *502* (7471), 359−363.
(12) Smith, J. N.; Barsanti, K. C.; Friedli, H. R.; Ehn, M.; Kulmala, M.; Collins, D. R.; Scheckman, J. H.; Williams, B. J.; McMurry, P. H. Observations of aminium salts in atmospheric nanoparticles and possible climatic implications. *Proc. Natl. Acad. Sci. U. S. A.* **2010**, *107* (15), 6634−6639.
(13) Li, Y.; Fu, T.-M.; Yu, J. Z.; Yu, X.; Chen, Q.; Miao, R.; Zhou, Y.; Zhang, A.; Ye, J.; Yang, X.; et al. Dissecting the contributions of organic nitrogen aerosols to global atmospheric nitrogen deposition and implications for ecosystems. *Nat. Sci. Rev.* **2023**, *10* (12), nwad244.
(14) Yao, L.; Wang, M. Y.; Wang, X. K.; Liu, Y. J.; Chen, H. F.; Zheng, J.; Nie, W.; Ding, A. J.; Geng, F. H.; Wang, D. F.; et al. Detection of atmospheric gaseous amines and amides by a high-resolution time-of-flight chemical ionization mass spectrometer with protonated ethanol reagent ions. *Atmos. Chem. Phys.* **2016**, *16* (22), 14527−14543.
(15) Long, B.; Xie, C.; Truhlar, D. G. Criegee Intermediates Compete Well with OH as a Cleaning Agent for Atmospheric Amides. *J. Am. Chem. Soc.* **2025**, *147* (25), 22237−22244.
(16) Wei, S.; Wan, Q.; Zhou, S.; Nie, W.; Chen, S. Spontaneous Generation of −CH2CN from Acetonitrile at the Air−Water Interface. *J. Am. Chem. Soc.* **2024**, *146* (47), 32777−32784.
(17) Bruno, A. G.; Harrison, J. J.; Chipperfield, M. P.; Moore, D. P.; Pope, R. J.; Wilson, C.; Mahieu, E.; Notholt, J. Atmospheric distribution of HCN from satellite observations and 3-D model simulations. *Atmos. Chem. Phys.* **2023**, *23* (8), 4849−4861.
(18) Ge, Y.; Liu, Y.; Chu, B.; He, H.; Chen, T.; Wang, S.; Wei, W.; Cheng, S. Ozonolysis of Trimethylamine Exchanged with Typical Ammonium Salts in the Particle Phase. *Environ. Sci. Technol.* **2016**, *50* (20), 11076−11084.
(19) Zhang, W.; Zheng, D.; Lao, J.; Li, R.; Chen, B.; Chen, J.; Zhong, J.; Ji, Y.; Li, G.; Francisco, J. S.; et al. Sulfate Promotes Amine Salt Ozonation in Atmospheric Aerosols. *J. Am. Chem. Soc.* **2025**, *147* (38), 34327−34338.
(20) Kanawade, V. P.; Jokinen, T. Atmospheric amines are a crucial yet missing link in Earth's climate via airborne aerosol production. *Commun. Earth Environ.* **2025**, *6* (1), 98.
(21) Karydis, V. A.; Tsimpidi, A. P.; Pozzer, A.; Lelieveld, J. How alkaline compounds control atmospheric aerosol particle acidity. *Atmos. Chem. Phys.* **2021**, *21* (19), 14983−15001.
(22) Yuan, B.; Koss, A. R.; Warneke, C.; Coggon, M.; Sekimoto, K.; de Gouw, J. A. Proton-Transfer-Reaction Mass Spectrometry: Applications in Atmospheric Sciences. *Chem. Rev.* **2017**, *117* (21), 13187−13229.
(23) Li, F.; Huang, D. D.; Liu, Q.; Tian, L.; Hoi, K. I.; Mok, K. M.; Li, Y. J. Measurement of Gaseous Nitrophenols and Their Precursors Using a Vocus Proton-Transfer-Reaction Time-of-Flight Mass Spectrometer (PTR-ToF-MS). *ACS ES T Air* **2025**, *2* (10), 2184−2194.
(24) VandeVondele, J.; Krack, M.; Mohamed, F.; Parrinello, M.; Chassaing, T.; Hutter, J. QUICKSTEP: Fast and accurate density functional calculations using a mixed Gaussian and plane waves approach. *Comput. Phys. Commun.* **2005**, *167* (2), 103−128.
(25) Kühne, T. D.; Iannuzzi, M.; Del Ben, M.; Rybkin, V. V.; Seewald, P.; Stein, F.; Laino, T.; Khaliullin, R. Z.; Schütt, O.; Schiffmann, F.; et al. CP2K: An electronic structure and molecular dynamics software package - Quickstep: Efficient and accurate electronic structure calculations. *J. Chem. Phys.* **2020**, *152*, 194103.
(26) Laio, A.; Parrinello, M. Escaping free-energy minima. *Proc. Natl. Acad. Sci. U. S. A.* **2002**, *99* (20), 12562−12566.
(27) Grimme, S. Semiempirical GGA-type density functional constructed with a long-range dispersion correction. *J. Comput. Chem.* **2006**, *27* (15), 1787−1799.
(28) Hartwigsen, C.; Goedecker, S.; Hutter, J. Relativistic separable dual-space Gaussian pseudopotentials from H to Rn. *Phys. Rev. B* **1998**, *58* (7), 3641−3662.
(29) Goedecker, S.; Teter, M.; Hutter, J. Separable dual-space Gaussian pseudopotentials. *Phys. Rev. B* **1996**, *54* (3), 1703−1710.
(30) Xia, D.; Chen, J.; Fu, Z.; Xu, T.; Wang, Z.; Liu, W.; Xie, H.-B.; Peijnenburg, W. J. G. M. Potential Application of Machine-Learning-Based Quantum Chemical Methods in Environmental Chemistry. *Environ. Sci. Technol.* **2022**, *56* (4), 2115−2123.
(31) Xu, Y.; Dong, X. N.; Xiao, H. Y.; Zhou, J. X.; Wu, D. S. Proteinaceous Matter and Liquid Water in Fine Aerosols in Nanchang, Eastern China: Seasonal Variations, Sources, and Potential Connections. *J. Geophys Res-Atmos.* **2022**, *127*, No. e2022JD036589.
(32) Zhang, Q.; Wang, Y.; Liu, M.; Zheng, M.; Yuan, L.; Liu, J.; Tao, S.; Wang, X. Wintertime Formation of Large Sulfate Particles in China and Implications for Human Health. *Environ. Sci. Technol.* **2023**, *57* (48), 20010−20023.
(33) Gong, K.; Ao, J.; Li, K.; Liu, L.; Liu, Y.; Xu, G.; Wang, T.; Cheng, H.; Wang, Z.; Zhang, X.; et al. Imaging of pH distribution inside individual microdroplet by stimulated Raman microscopy. *Proc. Natl. Acad. Sci. U. S. A.* **2023**, *120* (20), No. e2219588120.
(34) Margarella, A. M.; Perrine, K. A.; Lewis, T.; Faubel, M.; Winter, B.; Hemminger, J. C. Dissociation of Sulfuric Acid in Aqueous Solution: Determination of the Photoelectron Spectral Fingerprints of H2SO4, HSO4−, and SO42− in Water. *J. Phys. Chem. C* **2013**, *117* (16), 8131−8137.
(35) Sander, R. Compilation of Henry's law constants (version 5.0.0) for water as solvent. *Atmos. Chem. Phys.* **2023**, *23* (19), 10901−12440.
(36) Wang, M.; Kong, W.; Marten, R.; He, X.-C.; Chen, D.; Pfeifer, J.; Heitto, A.; Kontkanen, J.; Dada, L.; Kürten, A.; et al. Rapid growth of new atmospheric particles by nitric acid and ammonia condensation. *Nature* **2020**, *581* (7807), 184−189.
(37) Tang, L.; Feng, Z.; Shang, D.; Zeng, L.; Wu, Z.; Wang, H.; Chen, S.; Li, X.; Zeng, L.; Hu, J.; et al. Ongoing uncoordinated anthropogenic emission abatement promotes atmospheric new particle growth in a Chinese megacity. *Nat. Commun.* **2025**, *16* (1), 6720.

Downloaded from pubs.acs.org/jacsat/article-pdf/doi/10.1021/jacs.6c10698/6872891/jacs.6c10698.pdf by GUANGDONG UNIV OF TECHNOLOGY user on 12 October 2026

https://doi.org/10.1021/jacs.6c10698
J. Am. Chem. Soc. XXXX, XXX, XXX−XXX